2020

Cloud shadows drive vertical migrations of deep-dwelling marine life

Melissa M. Omand

Deborah K. Steinberg
Virginia Institute of Marine Science

Karen Stamieszkin
Virginia Institute of Marine Science

Cloud shadows drive vertical migrations of deep-dwelling marine life

Melissa M. Omand[a,1], Deborah K. Steinberg[b], and Karen Stamieszkin[b]

[a]Graduate School of Oceanography, University of Rhode Island, Narragansett, RI 02882; and [b]Biological Sciences Department, Virginia Institute of Marine Science, Gloucester Point, VA 23062

Edited by David M. Karl, University of Hawaii at Manoa, Honolulu, HI, and approved June 28, 2021 (received for review November 3, 2020)

Many zooplankton and fishes vertically migrate on a diel cycle to avoid predation, moving from their daytime residence in darker, deep waters to prey-rich surface waters to feed at dusk and returning to depth before dawn. Vertical migrations also occur in response to other processes that modify local light intensity, such as storms, eclipses, and full moons. We observed rapid, high-frequency migrations, spanning up to 60 m, of a diel vertically migrating acoustic scattering layer with a daytime depth of 300 m in the subpolar Northeastern Pacific Ocean. The depth of the layer was significantly correlated, with an ∼5-min lag, to cloud-driven variability in surface photosynthetically available radiation. A model of isolume-following swimming behavior reproduces the observed layer depth and suggests that the high-frequency migration is a phototactic response to absolute light level. Overall, the cumulative distance traveled per day in response to clouds was at least 36% of the round-trip diel migration distance. This previously undescribed phenomenon has implications for the metabolic requirements of migrating animals while at depth and highlights the powerful evolutionary adaptation for visual predator avoidance.

vertical migration | zooplankton | phototaxis | clouds

Aquatic organisms, including species of zooplankton and fish, migrate vertically in the world's lakes and oceans on daily and seasonal timescales. The daily movement—termed diel vertical migration, or DVM—is one of the most ubiquitous animal behavioral phenomena observed in aquatic ecology and, since first described over 200 y ago (1), has been the subject of >3,000 published studies. There is general consensus that DVM is a predator avoidance behavior, whereby migrators rise to the water's surface to feed on sunlight-fueled phytoplankton and zooplankton at night and descend to the darker mesopelagic "twilight zone" to avoid being consumed by visual predators during the day (2, 3). Sunlight is the primary cue for this behavior down to depths where organisms can no longer detect it (4, 5), with migrators arriving at the sea surface within less than an hour after sunset and departing less than an hour before sunrise globally (6). Migratory organisms can respond to light from sources other than the sun, such as moonlight (7–9) and anthropogenic light (10, 11). Furthermore, zooplankton alter their DVM in response to chemicals produced by fish, called kairomones (12, 13), and to internal circadian rhythms that can cue migration during periods of polar midnight sun (14). DVM is not only important to understanding aquatic trophic dynamics, but it also impacts nutrient cycles worldwide, as organic matter consumed at the surface by migrators is transported to depth, metabolized, and released as dissolved inorganic carbon (respired), dissolved organic matter (excreted), and particulate organic matter (egested) (15–18).

Relatively little attention has been paid to the daytime phototactic behavior of migratory organisms at depth. Kaartvedt et al. (19) showed that mesopelagic fish swam upward beneath a passing storm, Frank and Widder (20) found that a transient influx of turbid water enhanced light attenuation and induced an upward migration of crustaceans and salps, and other studies show that cloudiness can influence vertical migration behavior on diel timescales (21–23). McLaren (24) proposed that during the day, zooplankton may be "resting" in deeper, cooler waters to save energy, and studies estimating migrator excretion and respiration rates at depth assume a constant rate of metabolic activity throughout daylight hours based largely on temperature and animal size (15, 18). In situ observations of inactivity by animals at depth are for mesopelagic fishes that are large enough to be observed by submersibles (24), while less information is available for zooplankton. Models that use the optimization of fitness (energy acquisition) versus mortality (predation) to simulate DVM behavior also assume that organisms are resting at depth with no variation in metabolic demand once daytime depths are reached (25–27), and some experimental results support this hypothesis (28).

Hydroacoustics record the high-resolution vertical distribution of migrators and are used to study many aspects of DVM behavior, including the timing of DVM (6, 29), the distribution of DVM layers in relation to oxygen minimum zones (30, 31), and the seasonality of DVM biomass (5, 29, 32). We use hydroacoustics to show that, contrary to previous assumptions, a deep sound-scattering layer (DSL) of migrating organisms are not resting at their daytime migration depths; rather, they are swimming constantly in response to cloud-driven light variations at the sea surface. Zooplankton and micronekton follow isolumes to their daytime residence depths (20, 33). We show that a DSL also tracks isolumes while at depth, resulting in high-frequency migrations (HFM) that could increase migrator metabolic demand in the mesopelagic zone.

Results

A site in the subarctic North Pacific Ocean near Ocean Station Papa (Station P; 145°W, 50°N, *SI Appendix*, Fig. S1) was occupied for 25 d in August–September 2018 as part of the EXport

Significance

Our study provides evidence that, in addition to diel vertical migration, zooplankton residing at >300-m depth during the day perform high-frequency, vertical migrations due to light modulation by clouds. Using a water-following framework and measurements and modeling of the twilight zone light field, we isolated the detailed phototactic response and show that some twilight zone animals are considerably more active than previously thought, with a cumulative distance traveled of more than one-third of that for diel migration. The increased movement increases predation risk and has implications for the metabolic requirements of these animals in the food-limited deep sea.

Author contributions: M.M.O. and D.K.S. designed research; M.M.O., D.K.S., and K.S. performed research; M.M.O. analyzed data; and M.M.O., D.K.S., and K.S. wrote the paper.

The authors declare no competing interest.

This article is a PNAS Direct Submission.

[1]To whom correspondence may be addressed. Email: momand@uri.edu.

This article contains supporting information online at https://www.pnas.org/lookup/suppl/doi:10.1073/pnas.2022977118/-/DCSupplemental.

Published August 4, 2021.

Processes in the Ocean from RemoTe Sensing (EXPORTS) field campaign (33). Ship-based surface photosynthetically available radiation (PAR_o) revealed high-frequency variability in light level associated with clouds passing overhead (6 of 25 d shown in Fig. 1*A*). Observations of downwelling irradiance integrated between 400 and 700 nm (PAR) from a profiling Wirewalker (WW) were used to determine a near-surface diffuse attenuation coefficient of 0.065 m^{-1} and confirm that the cloud-driven variability extended throughout the euphotic zone (Fig. 1*B*). Modeled PAR (*SI Appendix*) below the euphotic zone was attenuated exponentially with a diffuse attenuation coefficient of 0.03 m^{-1} (Fig. 1 *C* and *D*). Numerous diel-migrating DSLs were observed in the acoustic Doppler current profiler (ADCP) backscatter anomalies, with the most distinct of these repeatedly descending to a maximum depth of about 300 m each day (Fig. 1*E*; *SI Appendix*, Fig. S2). The layer showed the classic signature of DVM, in addition to rapid daytime oscillations that span up to 60 m. Overall, we found that the DSL closely followed the 0.001 $\mu mol \cdot m^{-2} \cdot s^{-1}$ isolume (compare the black and white contours in Fig. 1*E*), an intensity that is at least four orders of magnitude above the reported photobehavioral sensitivity of mesopelagic crustaceans (35).

Correlation between High-Frequency Anomalies in PAR_o and DSL Depth. A selection of daytime records of high-pass filtered PAR_o' (black lines) and DSL′ (red lines) from the 25 d analyzed are shown in Fig. 2, *A*–*G*. Methods for extracting the DSL at 1 m vertical resolution is described in the *SI Appendix*. By high-pass filtering, we are excluding any variation due to diel fluctuations, leaving only variability occurring on scales less than 4 h (see *Materials and Methods*). These selected days represent a range of conditions when the PAR_o' variability was relatively large, spanning up to 1,000 $\mu mol \cdot m^{-2} \cdot s^{-1}$ (e.g., year days 232 and 243), and small (e.g., year days 226 and 231). Overall, a strong correlation was observed between DSL' and PAR_o'; however, we also show some examples when the correlation was low (year days 234 and 242). It appears that for these weakly correlated cases, PAR_o' fluctuated rapidly, with a period of ~10 min or less, and the DSL was not "keeping up." In general, DSL' lagged behind the fluctuations in PAR_o', with a maximum correlation occurring at a lag of 4 to 5 min (Fig. 2, *H*–*N*).

Over the course of the experiment, 20 of 25 d showed a significant correlation between DSL' and PAR_o' (black points, Fig. 3*A*). The correlation slightly increased upon introducing a temporal lag between the two-time series (gray points, Fig. 3*A*). The optimal lag time (highest r^2) varied between 1.9 and 7.2 min, with an average of 4.4 min (Fig. 3*B*). We conclude from this analysis that zooplankton and micronekton comprising the DSL were responding to short-term variability in the ambient light field by swimming up when the sky darkened and down when the sun reemerged. However, from our perspective on the ship, every day of the cruise was overcast, gray, and drizzly. The variations in PAR_o' were driven not by alternate periods of direct sunlight and cloud shadow but rather by a thick lower layer of clouds intermittently occluding a brighter upper layer of clouds. This suggests that the cloud-driven variations in the DSL (i.e., HFM) are likely not confined to blue sky and cumulus conditions.

Modeling HFM Swimming Behavior. This dataset provides an opportunity to examine in situ swimming behavior of mesopelagic organisms and hypotheses concerning cues for phototactic behavior in the animals that comprise the DSL. Here, we find that variations in the depth of the DSL are very well predicted by a simple phototactic model as follows: If the PAR at the DSL is at least 10% lower than a target isolume (0.001 $\mu mol \cdot m^{-2} \cdot s^{-1}$), then the layer swims up at a constant speed. If the PAR at the DSL is at least 10%

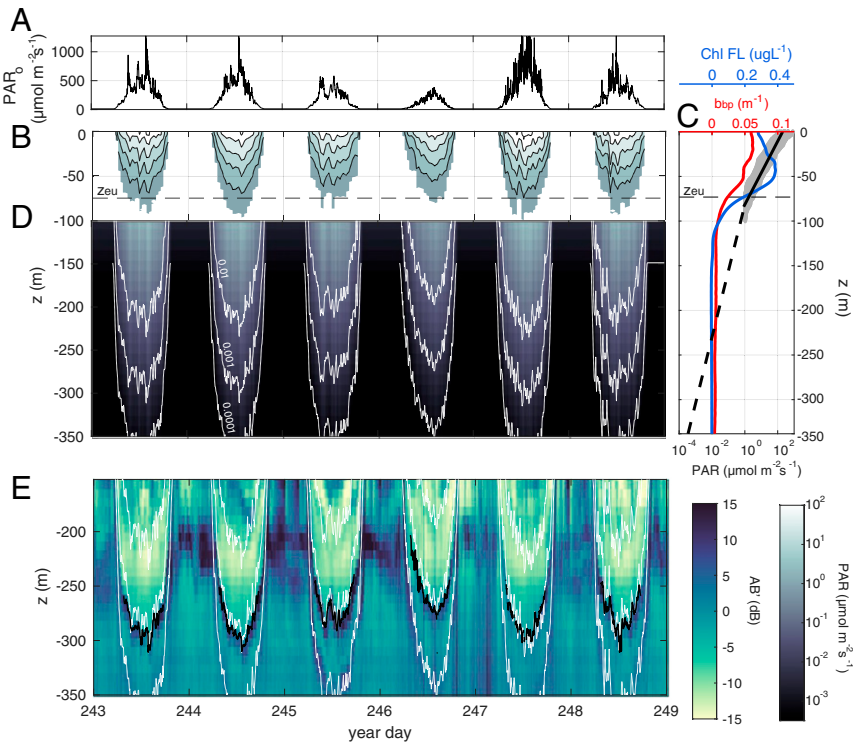

Fig. 1. Time series of (*A*) surface PAR_o measured from the R/V *Revelle* and (*B*) PAR depth profile (PAR_z) measured from the WW (white space indicates regions where data were removed when the sensor measured below its noise floor of 1 $\mu mol \cdot m^{-2} \cdot s^{-1}$). (*C*) WW PAR_z profiles collected between 1000 and 1400 local time (gray points) were fit to estimate the light attenuation coefficient in the euphotic zone, k_{eu} = 0.065 m^{-1}, with a 1% light level (horizontal dashed line), z_{eu}, of 71 m occurring just below declines in the average Chl a fluorescence (blue line) and optical backscatter (red line). The average PAR predicted from the twilight zone light attenuation coefficient k_{tz} = 0.03 m^{-1} is shown as a dashed black line. (*D*) Modeled PAR between 100 and 350 m. (*E*) AB′ with isolumes (white contours) and the DSL (black lines). See also *SI Appendix*, Fig. S2 for the layers evident in the raw AB signal.

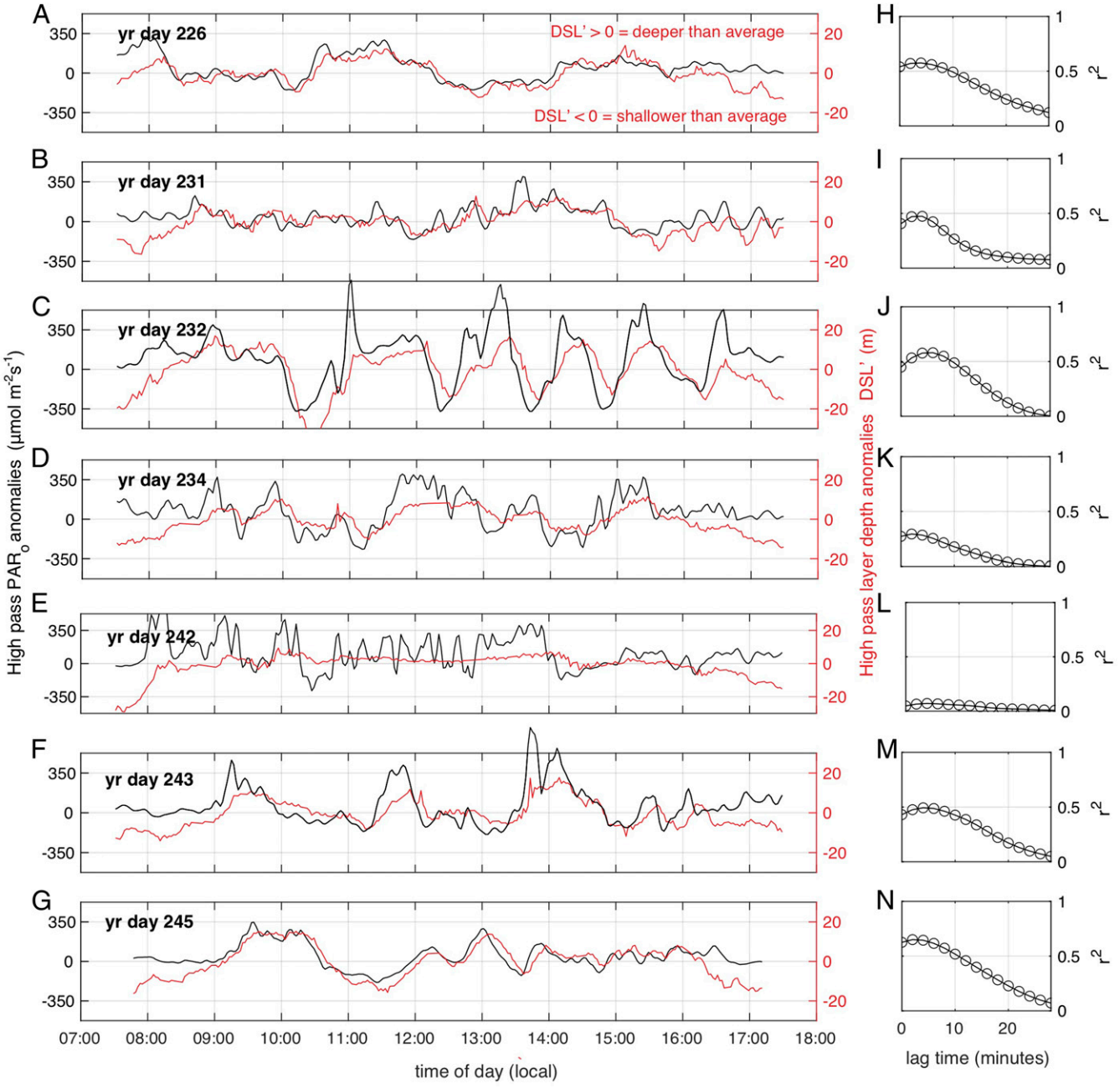

Fig. 2. (*A–G*) Selected daytime time series of the high-pass filtered anomalies of surface PAR_o' (black) and the DSL' (red). (*H–N*) The correlations (r^2) versus time lag between PAR_o' and DSL'. In each case, the maximum correlation occurs when DSL' is lagged behind PAR_o' by ~4 min (see Fig. 3*B*).

higher than the target isolume, then the layer swims down. Otherwise, the migrators stay in place. In equation form, this is

$$w_{swim} = \begin{Bmatrix} 2\ \text{cm}^{-1}, & \text{if } PAR_{mod}(zDSL) < 0.0009\ \mu\text{mol m}^{-2}\text{s}^{-1} \\ -2\ \text{cm}^{-1}, & \text{if } PAR_{\text{mod}}(zDSL) < 0.0011\ \mu\text{mol m}^{-2}\text{s}^{-1} \\ 0, & \text{otherwise} \end{Bmatrix}. \quad [1]$$

The swimming speed of 2 cm · s^{-1} was determined recursively by applying a range of swimming speeds and finding one that best matched the observations. This speed appears to be well within the swimming capability of these organisms, since they covered at least 200 m over ~1 h at dawn and dusk each day (a swimming speed of ~5 cm · s^{-1}), which is the same order of magnitude as the 7 cm · s^{-1} mean DVM swimming speed reported from a global dataset of acoustic backscatter (AB) (6). The simple phototactic swimming model resulted in a predicted migrator layer depth that was markedly more correlated with DSL' than PAR_o' and was significant for all days, with r^2 ranging from 0.4 to 0.95 (magenta points, Fig. 3*A*). An example of the layer depth predicted by the model is shown in Fig. 4*C* (compare the magenta and black lines). The model successfully captures many features of the DSL depth, such as the temporal lag relative to PAR and suppressed response to rapid variations in PAR (such as that occurring at 1040 hours, Fig. 4*C*).

Discussion

Light is the primary physical attribute governing the vertical distribution of plants and animals in the sea. Yet, the ways in

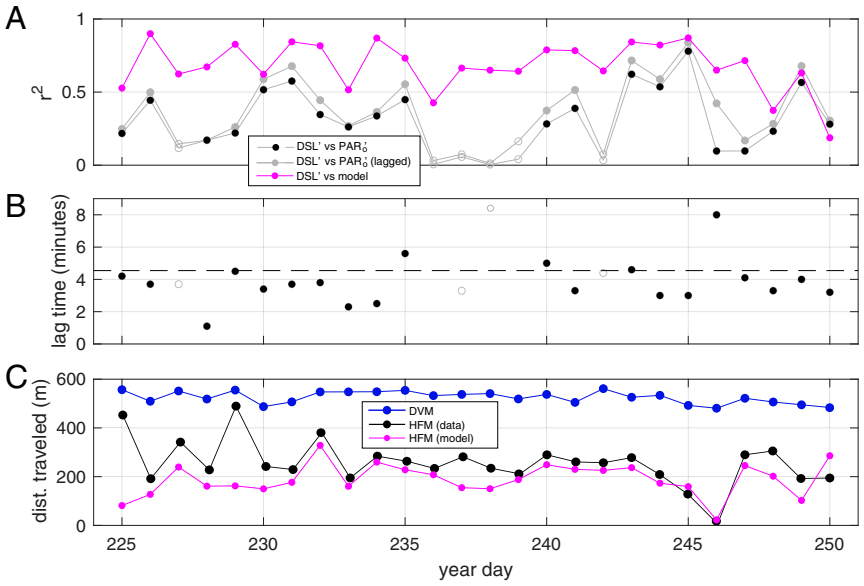

Fig. 3. Daily statistics and distance traveled per day by the migrators. (*A*) The r^2 correlations between PAR_o' and DSL′ at zero lag (black dots) and optimal lag (gray dots). Magenta dots indicate the correlation between the high-pass DSL′ and the high-pass modeled layer depth anomaly according to Eq. **1**. Points with insignificant correlation ($P > 0.001$) are plotted as open circles. The marked improvement in correlation by the model (even on year days 236–239) occurs because the model captures the lagged response, and smoothes over the most rapid changes in isolume depth. (*B*) Lag times between PAR_o' and DSL′ determined by the maximum correlation as indicated on the right-hand column on Fig. 2. (*C*) Cumulative distance traveled each day during DVM (estimated from AB′, blue points) and due to cloud-driven HFM (derived from the DSL′ [black] and modeled layer depth [magenta] points). The distance traveled each day due to DVM between the mixed layer (at night) and depth (during day) was calculated from the low-pass–filtered time series from Eq. **2** and the distance traveled due to HFM between 0700 and 1700 each day was estimated by integrating the changes in layer depth.

which light governs behavior or is otherwise used by animals in the vast habitat of the ocean's twilight zone is only just becoming understood (36). Here, we primarily use tools found on most research vessels (incident PAR and hull mounted ADCP) to identify an HFM behavior, and suggest that other archived vessel data may contain similar patterns. We found a strong correlation between cloud-induced light variability and a phototactic swimming response by animals that reside near 300 m during the daytime phase of their DVM. The migrators were detected with a 150-kHz ADCP, which suggests they were primarily zooplankton and micronekton (37–40) as opposed to larger fishes. Multiple Opening/Closing Net and Environmental Sensing System tows conducted in day–night pairs throughout the cruise revealed a daytime biomass maximum between 300- and 400-m depth composed mainly of organisms >2 mm (*SI Appendix*, Fig. S5*A*). Most of the zooplankton in this size class exhibited strong DVM behavior, including large calanoid copepods like *Metridia* spp., ostracods, salps, and euphausiids (*SI Appendix*, Fig. S5 *B–D*). Of these taxa, the latter is more typically associated with backscatter at this frequency (37–40), although salp chains are also readily detected at 120 and 200 kHz (41). Other likely targets at 150 kHz include siphonophores or small myctophids (not sampled as quantitatively with our net tows due to damage and net avoidance, respectively) and large amphipods and pteropods (37–40). The isolume-following behavior of these zooplankton and micronekton was well predicted by a phototactic model that prescribed a vertical swimming direction according to a binary light intensity measure (lighter/darker than target). The simplicity of this response in the context of presumed pressure to conserve energy for DVM, reproduction, and foraging is notable. Future studies should consider any advantages to HFM that might offset these costs. For example, as twilight zone light has a similar wavelength range to bioluminescence (440 to 515 nm) (42–44), animals such as euphausiids using bioluminescent countershading could benefit by more easily matching light produced by their photophores with ambient light if following an isolume. Also notable is the robustness of the HFM response we observed despite the uncertainty introduced by extrapolating incident and shallower water light measurements to depth (reviewed in ref. 36). Here, since these organisms returned to the same depth (*SI Appendix*, Fig. S2) and oxygen environment each day, the relatively clear water and repeated measurements in the water-following sampling framework of the EXPORTS campaign greatly enhanced our ability to isolate this phototactic response.

Through modeling HFM, we are able to evaluate two primary hypotheses concerning what aspect of the light field triggers migration [reviewed in Cohen and Forward 2009 (44)]. The "rate of change hypothesis" states that migrations are triggered by the rate and direction of change in light intensity and that there is a minimum relative rate of change detectable by migrators to prevent unnecessary vertical movement; this hypothesis has been supported by field studies (45–47). The "preferendum hypothesis" states that animals remain within a preferred light zone (isolume). Many organisms that comprise DSLs follow isolumes (48–51), but some organisms do not (23, 52, 53). These contradictory findings may be due to different species and behaviors, physical characteristics of the water column, vertical predator and prey distributions, and uncertainty around light intensity measurements in the twilight zone. We demonstrate here that the behavior of animals that constitute the DSL we observed is most consistent with the preferendum hypothesis—not only as a cue for DVM but also for HFM by seeking that isolume even as clouds pass overhead. However, it is also plausible that the cue to swim up or down may be triggered by a change in detected light. There is no indication that these organisms' ability to detect change in the light field is preventing HFM, with vertical movement occurring during the day in response to relative changes in ambient PAR up to 2× faster than the maximum relative changes observed at dawn and dusk (*SI Appendix*, Fig. S6). Furthermore, HFM occurs in the presence of internal waves that cause layer depth fluctuations of comparable size to the vertical fluctuations of the isolumes, suggesting that the animals swim to keep up with

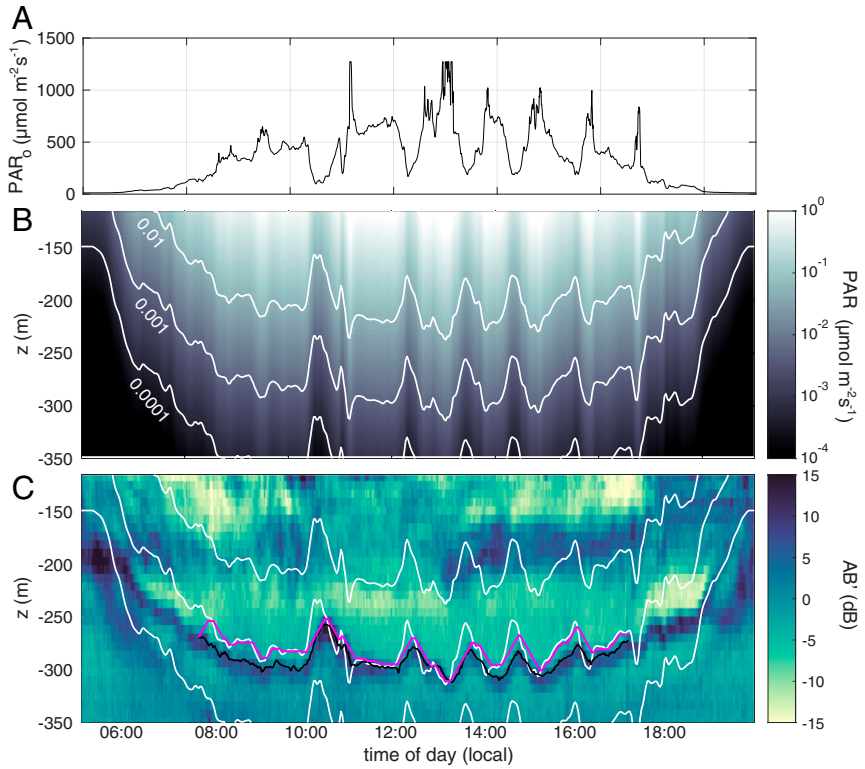

Fig. 4. Time series for year day 232 (following Fig. 1) of (*A*) surface PAR$_o$, (*B*) modeled PAR between 100- and 350-m depth, and (*C*) AB′ with contours of PAR (white lines) and the DSL (black lines). The magenta line indicates the depth variation predicted by a phototactic swimming model (Eq. **1**). The model reproduces the amplitude of the observed DSL fluctuations, the time lag between the two parameters, and the suppressed response to sharp or rapid fluctuations in the isolume.

cloud-driven light fluctuations while also compensating for internal wave-induced velocities. Internal waves occur over a range of timescales that span from the Coriolis (set by latitude, ∼16 h at our site) to the Brunt Vaisala frequency (set by the local density gradient [∼30 min] near 300-m depth in these observations). Near the depth of the DSL, the superinertial isopycnal oscillations measured by the WW were dominated by internal waves that were comparable in magnitude to the daytime DSL excursions (*SI Appendix*, Fig. S7). At 300 m below the surface, there is no feasible mechanism that would cause isopycnals and isolumes to consistently covary. The strong DSL–isolume correspondence demonstrates that the DSL variations are not caused by internal waves. In fact, in order to maintain such strict adherence to an isolume, we posit that the animals are able to swim in response to cloud-driven light variations and additionally compensate for the vertical water velocities induced by internal waves. Here, internal wave displacements roughly doubled the swimming distance needed to track the target isolume, suggesting that animals' energy requirement for HFM likely exceeds that predicted by our isolume-following model.

The energetic implications of HFM can be approximated by integrating the distance traveled due to diel and cloud-driven light variations, respectively (Fig. 3*C*). On days that are more overcast, the maximum migration depth is about 25 m less than on brighter days (e.g., year day 246 in Fig. 1). Overall, however, the distance traveled due to DVM was relatively consistent, with an average of about 530 m (e.g., black and magenta points, Fig. 3*C*). In contrast, the distance traveled due to HFM varied more widely depending on the cloud patterns above. Overall, a prediction based on the modeled behavior was lower than that obtained with the observed DSL because the model is derived solely from the ambient light field and excludes depth variability due to isopycnal motions. We find that by using the more conservative modeled estimate, the HFM distance traveled was at most about 70% of the DVM distance (year day 232) and that, on average, the HFM distance was about 36% of the round trip DVM distance.

It has long been posited that the ecological/evolutionary advantage of avoiding predation outweighs the energy expenditure of DVM. Indeed, this also appears applicable to HFM, as the animals that constitute the scattering layer observed here are also swimming constantly at their mesopelagic daytime residence depths. The implications are that energy expenditure in the mesopelagic zone for the migrating zooplankton community, and thus both the carbon requirements to meet their energetic demands and the vertical transport of carbon from surface to depth, may be higher than currently estimated using allometric relationships based on animal size and temperature (16, 54, 55). Other metrics of metabolism such as Electron Transport System, which measures respiration potential, may incorporate metabolic demands of HFM behavior, but each comes with its own uncertainties (56). It is clear that migration happens at multiple scales, and, subsequently, the redistribution of carbon and nutrients that is typically ascribed to the larger-scale DVM is also likely to occur at small scales due to HFM.

In conclusion, vertical migration is considerably more dynamic than previously thought. The observations presented here were made under overcast conditions with comparatively little cloud-driven variability. Settings with intermittent clouds and otherwise clear skies are likely to induce even larger amplitude cloud-driven vertical migrations. Animal behavior varies by species and is influenced by both biotic and abiotic factors that change with depth and season and by region. While we concentrated our analysis on a single DSL, we detected daytime HFM in multiple

DSLs. We therefore suggest that this behavior could be widespread, occurring in other regions and throughout the twilight zone, which can be evaluated in subsequent studies.

Materials and Methods

Data were collected from the R/V *Revelle* during the 2018 EXPORTS field campaign (34) between August 12 and September 10 near Ocean Station Papa (145°W, 50°N) (gray lines, *SI Appendix*, Fig. S1). This study utilizes three data types: 1) ship-mounted surface PAR_o (Biospherical QSR-2200, *SI Appendix*, Fig. S2*A*), 2) acoustic backscatter (AB) intensity from the hull-mounted narrowband 150-kHz ADCP (RD Instruments, *SI Appendix*, Fig. S2*B*), and 3) profiles from a WW. Anomalies in AB (*AB′*) were calculated by subtracting the signal from the time-averaged ADCP backscatter along an isobar (*SI Appendix*, Eq. 5), such that positive values of *AB′* indicate higher-than-average scattering at that depth (see Fig. 1*E*). The depth of a prominent DSL at 300 m (daytime) was detected by objectively mapping *AB′* (8-m bins) onto a finer vertical scale for each 2-min time interval and finding, to the closest 1 m, the local maximum in *AB′* between 210 and 350 m (*SI Appendix*). High-frequency variations in PAR were detected from the ship-mounted surface PAR sensor and onboard a drifting wave-powered WW profiler (57) equipped with a conductivity, temperature, depth instrument (RBR Maestro), chlorophyll-*a* fluorescence and optical backscatter sensors (WetLabs ECOtriplet), and PAR_z (JFE Advantech DEFI-L). Over the course of the cruise, the WW (red lines, *SI Appendix*, Fig. S1) was repositioned three times at roughly 8-d intervals near a Lagrangian float. The R/V *Revelle* followed the drifting assets, generally staying within 4 km (gray lines, *SI Appendix*, Fig. S1). The Lagrangian framework of this experiment contributed substantially to our ability to isolate high-frequency motions of the DSL from other sources of variability.

High-frequency oscillations in the DSL were isolated by computing, and then subtracting, a low-pass signal from the DSL time series (calculated with a running median window of 4 h). High-frequency variations in surface PAR_o and in the modeled layer depth were determined in the same fashion. The correlation analysis shown in Fig. 3*A* was applied strictly to the high-pass filtered data and model output to eliminate any residual correlations due to DVM and the diel light cycle.

$$DSL' = DSL - DSL_{lp} \text{ and } PAR_o' = PAR_o - PAR_{olp}. \quad [2]$$

The resulting anomalies in measured DSL′, PAR_o′, and modeled DSL′ exclude diel variation, preserving only variability that occurs over time periods less than 4 h. We evaluated two hypotheses regarding cues for vertical migration in marine organisms. The "preferendum hypothesis" was evaluated by correlating the high-pass–filtered PAR and the high-pass–filtered DSL depth (see *SI Appendix* for details). The "rate-of-change hypothesis" was evaluated by comparing the relative rate of change in light intensity at 380 m throughout the day when HMF was taking place to the rate of change at dawn and dusk (see *SI Appendix* for details).

Data Availability. All EXPORTS data are available through the SeaBASS (DOI: 10.5067/SeaBASS/EXPORTS/DATA001) and R2R (DOI: 10.7284/908060) data repositories.

ACKNOWLEDGMENTS. Funding for this work was provided by NASA Grants 80NSSC17K0662, 80NSSC18K1323, and 80NSSC17K0654 as a component of the EXport Processes in the Ocean from RemoTe Sensing (EXPORTS) research program. Thanks to the captain and crew of the R/V *Roger Revelle* for smooth at-sea operations.

1. G. Cuvier, *Le règne animal* (Masson, Paris, 1817).
2. W. Lampert, The adaptive significance of diel vertical migration of zooplankton. *Funct. Ecol.* **3**, 21–27 (1989).
3. G. C. Hays, A review of the adaptive significance and ecosystem consequences of zooplankton diel vertical migrations. *Hydrobiologia* **503**, 163–170 (2003).
4. R. B. Forward Jr, Diel vertical migration: Zooplankton photobiology and behaviour. *Oceanogr. Mar. Biol. Annu. Rev.* **26**, 1–393 (1988).
5. H. van Haren, T. J. Compton, Diel vertical migration in deep sea plankton is finely tuned to latitudinal and seasonal day length. *PLoS One* **8**, e64435 (2013).
6. D. Bianchi, K. A. S. Mislan, Global patterns of diel vertical migration times and velocities from acoustic data. *Limnol. Oceanogr.* **61**, 353–364 (2016).
7. J. Ochoa, H. Maske, J. Sheinbaum, J. Candela, Diel and lunar cycles of vertical migration extending to below 1000 m in the ocean and the vertical connectivity of depth-tiered populations. *Limnol. Oceanogr.* **58**, 1207–1214 (2013).
8. K. S. Last, L. Hobbs, J. Berge, A. S. Brierley, F. Cottier, Moonlight drives ocean-scale mass vertical migration of zooplankton during the Arctic Winter. *Curr. Biol.* **26**, 244–251 (2016).
9. G. A. Tarling, F. Buchholz, J. B. L. Matthews, The effect of lunar eclipse on the vertical migration behaviour of Meganyctiphanes norvegica (Crustacea: Euphausiacea) in the Ligurian Sea. *J. Plankton Res.* **21**, 1475–1488 (1999).
10. M. Ludvigsen *et al*., Use of an autonomous surface vehicle reveals small-scale diel vertical migrations of zooplankton and susceptibility to light pollution under low solar irradiance. *Sci. Adv.* **4**, eaap9887 (2018).
11. J. Berge *et al*., Artificial light during the polar night disrupts Arctic fish and zooplankton behaviour down to 200 m depth. *Commun. Biol.* **3**, 102 (2020).
12. J. Ringelberg, The photobehaviour of Daphnia spp. as a model to explain diel vertical migration in zooplankton. *Biol. Rev. Camb. Philos. Soc.* **74**, 397–423 (1999).
13. J. Cohen, R. B. Forward, Photobehavior as an inducible defense in the marine copepod Calanopia americana. *Limnol. Oceanogr.* **50**, 1269–1277 (2005).
14. L. Hüppe *et al*., Evidence for oscillating circadian clock genes in the copepod *Calanus finmarchicus* during the summer solstice in the high Arctic. *Biol. Lett.* **16**, 20200257 (2020).
15. D. K. Steinberg *et al*., Zooplankton vertical migration and the active transport of dissolved organic and inorganic carbon in the Sargasso Sea. *Deep Sea Res. Part I Oceanogr. Res. Pap.* **47**, 137–158 (2000).
16. H. Al-Mutairi, M. R. Landry, Active export of carbon and nitrogen at Station ALOHA by diel migrant zooplankton. *Deep Sea Res. Part II Top. Stud. Oceanogr.* **48**, 2083–2103 (2001).
17. S. Hernández-León *et al*., Zooplankton and micronekton active flux across the tropical and subtropical Atlantic Ocean. *Front. Marine Sci.* **6**, 535. (2019).
18. L.E. Kwong, N. Henschke, E.A. Pakhomov, J.D. Everett, I.M. Suthers, Mesozooplankton and micronekton active carbon transport in contrasting eddies. *Front. Marine Sci.* **6**, 825 (2020).
19. S. Kaartvedt, A. Røstad, D. L. Aksnes, Changing weather causes behavioral responses in the lower mesopelagic. *Mar. Ecol. Prog. Ser.* **574**, 259–263 (2017).
20. T. M. Frank, E. Widder, Effects of a decrease in downwelling irradiance on the daytime vertical distribution patterns of zooplankton and micronekton. *Mar. Biol.* **140**, 1181–1193 (2002).
21. J. M. Pinot, J. Jansá, Time variability of acoustic backscatter from zooplankton in the Ibiza Channel (western Mediterranean). *Deep Sea Res. Part I Oceanogr. Res. Pap.* **48**, 1651–1670 (2001).
22. E. Potiris *et al*., Acoustic Doppler current profiler observations of migration patterns of zooplankton in the Cretan Sea. *Ocean Sci.* **14**, 783–800 (2018).
23. S. M. Parra *et al*., Acoustic detection of zooplankton diel vertical migration behaviors on the northern Gulf of Mexico shelf. *Limnol. Oceanogr.* **64**, 2092–2113 (2019).
24. I. A. McLaren, Effects of temperature on growth of zooplankton, and the adaptive value of vertical migration. *J. Fisheries Board Canada* **20**, 685–727 (1963).
25. E. G. Barham, Deep-sea fishes: lethargy and vertical orientation. In *Proceedings of an International Symposium on Biological Sound Scattering in the Ocean*, G. B. Farquhar, Ed. (U.S. Government Printing Office, Washington, DC, 1971), pp. 100–118.
26. A. de Robertis, Size-dependent visual predation risk and the timing of vertical migration: An optimization model. *Limnol. Oceanogr.* **4**, 10.4319/lo.2002.47.4.0925 (2002).
27. A. N. Hansen, A. W. Visser, Carbon export by vertically migrating zooplankton: An optimal behavior model. *Limnol. Oceanogr.* **61**, 701–710 (2016).
28. D. W. Chess, J. A. Stanford, Experimental effects of temperature and prey assemblage on growth and lipid accumulation by Mysis relicta loven. *Hydrobiologia* **412**, 155–164 (1999).
29. S. Jiang, T. D. Dickey, D. K. Steinberg, L. P. Madin, Temporal variability of zooplankton biomass from ADCP backscatter time series data at the Bermuda Testbed Mooring site. *Deep Sea Res. Part I Oceanogr. Res. Pap.* **54**, 608–636 (2007).
30. T. A. Klevjer, D. J. Torres, S. Kaartvedt, Distribution and diel vertical movements of mesopelagic scattering layers in the Red Sea. *Mar. Biol.* **159**, 1833–1841 (2012).
31. D. Bianchi, E. D. Galbraith, D. A. Carozza, K. Mislan, C. A. Stock, Intensification of open-ocean oxygen depletion by vertically migrating animals. *Nat. Geosci.* **6**, 545–548 (2013).
32. B. Cisewski, V. H. Strass, M. Rhein, S. Krägefsky, Seasonal variation of diel vertical migration of zooplankton from ADCP backscatter time series data in the Lazarev Sea, Antarctica. *Deep Sea Res. Part I Oceanogr. Res. Pap.* **57**, 78–94 (2010).
33. K. J. Heywood, Diel vertical migration of zooplankton in the Northeast Atlantic. *J. Plankton Res.* **18**, 163–184 (1996).
34. D. A. Siegel *et al*., An operational overview of the EXport Processes in the Ocean from RemoTe Sensing (EXPORTS) Northeast Pacific field deployment. *Elem. Sci. Anth.* **9**, 10.1525/elementa.2020.00107 (2021).
35. T. J. Myslinkski, T. M. Frank, E. A. Widder, Correlation between photosensitivity and downwelling irradiance in mesopelagic crustaceans. *Mar. Biol.* **147**, 619–629 (2005).
36. S. Kaartvedt, T. J. Langbehn, D. L. Aksnes, Enlightening the ocean's twilight zone. *ICES J. Mar. Sci.* **76**, 803–812 (2019).
37. A. C. Lavery *et al*., Determining dominant scatterers of sound in mixed zooplankton populations. *J. Acoust. Soc. Am.* **122**, 3304–3326 (2007).
38. H. S. La *et al*., Zooplankton and micronekton respond to climate fluctuations in the Amundsen Sea polynya, Antarctica. *Sci. Rep.* **9**, 10087 (2019).
39. K. J. Benoit-Bird, G. L. Lawson, Ecological insights from pelagic habitats acquired using active acoustic techniques. *Annu. Rev. Mar. Sci.* **8**, 463–490 (2016).
40. M. H. Radenac, P. E. Plimpton, A. Lebourges-Dhaussy, L. Commien, M. J. McPhaden, Impact of environmental forcing on the acoustic backscattering strength in the equatorial Pacific: Diurnal, lunar, intraseasonal, and interannual variability. *Deep Sea Res. Part I Oceanogr. Res. Pap.* **57**, 1314–1328 (2010).

41. P. H. Wiebe *et al*., The acoustic properties of Salpa thompsoni. *ICES J. Mar. Sci.* **67**, 583–593 (2010).
42. T. M. Frank, E. A. Widder, UV light in the deep-sea: in situ measurement of downwelling irradiance in relation to the visual threshold sensitivity of UV-sensitive crustaceans. *Mar. Freshwat. Behav. Physiol.* **27**, 189–197 (1996).
43. E. A. Widder, Bioluminescence and the pelagic visual environment. *Mar. Freshwat. Behav. Physiol.* **35**, 1–26 (2002).
44. J. H. Cohen, R. B. Forward Jr, Zooplankton diel vertical migration—a review of proximate control. *Oceanogr. Mar. Biol.* **47**, 77–109 (2009).
45. D. E. Stearns, R. B. Forward Jr, Copepod photobehavior in a simulated natural light environment and its relation to nocturnal vertical migration. *Mar. Biol.* **82**, 91–100 (1984).
46. R. B. Forward Jr, Behavioral responses of larvae of the crab Rhithropanopeus harrisii (Brachyura: Xanthidae) during diel vertical migration. *Mar. Biol.* **90**, 9–18 (1985).
47. J. Ringelberg, Enhancement of the phototactic reaction in Daphnia hyalina by a chemical mediated by juvenile perch (Perca fluviatilis). *J. Plankton Res.* **13**, 17–25 (1991).
48. E. M. Kampa, B. P. Boden, Submarine illumination and the twilight movements of a sonic scattering layer. *Nature* **174**, 869 (1954).
49. B. Baliño, D. L. Aksnes, Winter distribution and migration of the sound scattering layers, zooplankton and micronekton in Masfjorden, western Norway. *Mar. Ecol. Prog. Ser.* **102**, 35–50 (1993).
50. E. Norheim, T. A. Klevjer, D. L. Aksnes, Evidence for light-controlled migration amplitude of a sound scattering layer in the Norwegian Sea. *Mar. Ecol. Prog. Ser.* **551**, 45–52 (2016).
51. L. Hobbs *et al*., A marine zooplankton community vertically structured by light across diel to interannual timescales. *Biol. Lett.* **17**, 20200810 (2021).
52. A. Valle-Levinson, L. Castro, M. Cáceres, O. Pizarro, Twilight vertical migrations of zooplankton in a Chilean fjord. *Prog. Oceanogr.* **129**, 114–124 (2014).
53. C. L. Charpentier, C. S. Angell, P. I. Duffy, J. H. Cohen, Natural variations in estuarine fish, fish odor, and zooplankton photobehavior. *Mar. Freshwat. Behav. Physiol.* **52**, 265–282 (2020).
54. D. K. Steinberg *et al*., Bacterial vs. zooplankton control of sinking particle flux in the ocean's twilight zone. *Limnol. Oceanogr.* **53**, 1327–1338 (2008).
55. T. Ikeda, Respiration and ammonia excretion by marine metazooplankton taxa: Synthesis toward a global-bathymetric model. *Mar. Biol.* **161**, 2753–2766 (2014).
56. S. Hernández-León, S. Calles, M. L. Fernández de Puelles, The estimation of metabolism in the mesopelagic zone: Disentangling deep-sea respiration. *Prog. Oceanogr.* **178**, 10.1016/j.pocean.2019.102163 (2019).
57. L. Rainville, R. Pinkel, Wirewalker: An autonomous wave-powered vertical profiler. *J. Atmos. Ocean. Technol.* **18**, 1048–1051 (2001).